Hydrodesulfurization of FeS^+: Predominance of Kinetic over Thermodynamic Control

Susanne Bärsch, Ilona Kretzschmar, Detlef Schröder, and Helmut Schwarz*

Institut für Organische Chemie der Technischen Universität Berlin, Strasse des 17. Juni 135, D-10623 Berlin, Germany

P. B. Armentrout*

Department of Chemistry, University of Utah, Salt Lake City, Utah 84112

Received: January 21, 1999; In Final Form: May 6, 1999

The reaction of FeS^+ with D_2 is examined by guided-ion beam mass spectrometry. Three products, Fe^+, FeD^+, and $FeSD^+$, are formed in endothermic processes, and thresholds for these reactions are determined. Comparison of the thresholds with literature thermochemistry reveals considerable activation barriers in excess of the endothermicities for the formation of Fe^+ and $FeSD^+$. Additional bracketing and equilibrium measurements in a Fourier transform ion-cyclotron resonance mass spectrometer yield $D_0(Fe^+-SH) = 66.0 \pm 2.6$ kcal/mol. A potential-energy surface of the system $[Fe,H_2,S]^+$ predicted by density functional theory is used to interpret the experimental data. According to these calculations, the lowest-energy path for Fe−S bond activation involves 1,2-addition of hydrogen across the Fe−S bond along with spin inversion from the sextet to the quartet surface.

Introduction

Transition-metal sulfides have attracted some attention in the development of catalysts for several chemical and petrochemical processes.[1] While the more common transition-metal oxides exhibit a greater reactivity, transition-metal sulfides are more resistant toward catalyst poisoning and often possess a greater selectivity as compared to their oxygen analogues.[2] In addition, the chemistry of sulfur and its transition-metal compounds is of great relevance in many biological and geological systems.[3] In biological systems, a variety of enzymes such as hydrogenases, nitrogenases, sulfite reductases, and others contain transition-metal sulfide building blocks in the active sites.[4] Among these enzymes, proteins with Fe_mS_n cores are of particular interest,[5] and the most prominent example of iron−sulfur enzymes is probably the cubic Fe_4S_4 core in ferredoxins. Other enzymes also contain FeS, Fe_2S_2, and Fe_3S_4 building blocks as well as heterometallic sulfide clusters.

Investigation of the chemistry of model systems at a molecular level is an important first step toward understanding the chemistry of the active sites of enzymes. Gas-phase experiments are well-established means for the investigation of both the intrinsic reactivity of organometallic systems and the role of electronic structures.[6] For example, they have been used extensively in the investigation of transition-metal oxides.[7,8] Despite the relevance of transition-metal sulfides, relatively few gas-phase studies have been carried out on these systems.[9−11] The FeS^+ cation investigated in this paper can be regarded as the smallest model system for larger iron−sulfur clusters. The prototype reaction of FeS^+ with molecular hydrogen is the simplest model for the chemical behavior of iron sulfide in σ-bond activation processes. Here, we report a study on the $[Fe,H_2,S]^+$ system using two advanced mass-spectrometric methods, i.e., the guided-ion beam (GIB) technique as well as Fourier transform ion-cyclotron resonance (FT-ICR), combined with a computational study using density functional theory (DFT).

Experimental Section

GIB. The guided-ion beam mass spectrometer used for the experiments has been described in detail previously.[12,13] Atomic Fe^+ ions are produced in a direct current discharge source[12c] connected to a flow tube.[12b] Inside the source, an iron cathode is held at 1.5−2.5 kV in a plasma consisting of about 90% helium and 10% argon. Ar^+ ions are produced in the discharge and accelerated toward the iron rod, thereby sputtering off neutral and ionic metal fragments. About 60 cm downstream from the discharge, FeS^+ is produced by adding carbonyl sulfide to the flow. In the remaining 40 cm of the flow tube, the ions undergo $>10^4$ thermalizing collisions at a typical flow tube pressure of ∼0.7 mbar. At the end of the flow tube, the ions are extracted, accelerated, and passed through a magnetic sector for reactant ion selection. The mass-selected ions are decelerated to the desired kinetic energies and focused into an rf octopole device. The octopole is used to trap the reactant and product ions in the radial direction and therefore maintains good collection efficiency at low kinetic energies. The octopole passes through a gas cell of known effective length (8.26 cm) filled with the neutral D_2 reactant. The neutral is present in the reaction cell at relatively low steady pressures of $(1-3) \times 10^{-4}$ mbar to ensure single collision conditions. Unreacted ions and product ions drift from the reaction cell to the end of the octopole and are extracted into a quadrupole mass filter for mass analysis and subsequent detection by a secondary electron/scintillation detector.

Laboratory ion energies (E_{lab}) are converted into center-of-mass energies (E_{CM}) using $E_{CM} = E_{lab}M/(M + m)$ where M and m are the corresponding reactant neutral and ion masses. The absolute energy scale and the corresponding full width at

10.1021/jp990244+ CCC: $18.00
Published on Web 07/14/1999

half-maximum (fwhm) of the ion beam kinetic energy distribution are determined as described in previous publications.[12] The beams have Gaussian kinetic energy distributions with an average fwhm of ca. 0.24 eV in the laboratory frame. The uncertainty of the absolute energy scale is ±0.05 eV (lab). Details for the conversion of raw ion intensities into cross sections have been outlined previously.[12a] Absolute cross sections are estimated to be correct within ±20%.

Data analysis has been performed as follows. Cross sections are modeled using eq 1,[12c,d] where E denotes the relative

$$\sigma(E) = \sigma_0 \sum g_i (E + E_i - E_0)^n / E \qquad (1)$$

translational energy, E_0 is the reaction threshold, σ_0 is an energy independent scaling factor, and n is a fitting parameter. The summation over rovibrational energy levels i with energies E_i and relative populations g_i explicitly includes the internal energies of polyatomic reactants. Relative populations g_i are obtained from a Maxwell−Boltzmann distribution of vibrational energy levels at 300 K, calculated using the Beyer−Swinehart algorithm.[13] The vibrational frequency of D_2 is taken from ref 14, and that of FeS^+ is calculated as 463 cm^{-1} at the B3LYP/6-311+G* level of theory (see below). After convolution of the model over the kinetic energy distributions of the reactants, the parameters σ_0, n, and E_0 are optimized to best reproduce the data using a least-squares criterion. Reported errors in E_0 comprise the range of values obtained for several data sets and the absolute uncertainty of the energy scale. Equation 1 inherently assumes that all of the internal energy is capable of coupling into the reaction coordinate, an assumption that has been shown to lead to accurate thermochemistry in numerous cases.[12c,d,15−17]

FT-ICR. The experiments are performed in a Spectrospin-CMS-47X Fourier transform ion-cyclotron resonance mass spectrometer described previously.[18] Briefly, the iron cations are generated using laser desorption/laser ionization from an iron target in the external ion source. The ions are extracted from the external ion source and transferred into the analyzer cell that is located in the field of a superconducting magnet (field strength ca. 7 T). The $^{56}Fe^+$ isotope is isolated using FERETS, a computer-controlled ion-ejection protocol that combines frequency sweeps and single frequency pulses to eject all undesired ions.[19] Iron halide cations FeX^+ (X = Cl, Br) are produced by reaction of the isolated Fe^+ ions with pulsed-in CH_3X.[26] $FeOH^+$ cations are generated by pulsing a mixture of N_2O and CH_4 into the reaction cell.[21,22] $FeSH^+$ is formed by reacting FeX^+ (X = OH, Cl) with hydrogen sulfide (see below). The ions of interest are mass-selected as described above and thermalized by collisions with argon prior to their ion−molecule reactions. Ion thermalization is monitored by the reproducibility of the reaction kinetics as well as the strict first-order behavior of the reactant ion decay.[22] To obtain satisfactory signal-to-noise ratios, 50−100 scans are accumulated. For the bracketing experiments, H_2S is admitted to the cell via a leak valve at a stationary pressure of approximately 5×10^{-9} mbar. The cell pressure is measured by a calibrated ion gauge (Balzers IMG070). Rate constants are determined from the pseudo-first-order decay of the reactant ion and converted to reaction efficiencies k/k_{capt} by comparison with the respective gas-kinetic collision rates (k_{capt}) determined by capture theory.[23] All functions of the mass spectrometer are controlled by a Bruker ASPECT 3000 minicomputer.

As described below, the reaction $FeCl^+ + H_2S \rightleftarrows FeSH^+ + HCl$ is reversible under FT-ICR conditions, thus allowing a thermochemical equilibrium to be established at an assumed temperature of 298 K.[22] To this end, $FeSH^+$ is trapped in mixtures of H_2S and HCl with different ratios of the two components (see below). The exchange reactions are monitored for several reaction times. Equilibrium is assumed to be established when the ratio of $FeCl^+$ to $FeSH^+$ is time independent.[24] The equilibrium constant K_{eq} is derived from the relative intensities (I_i) of the product ions and the absolute pressures (p_i) of the neutral reactants (eq 2). The error of the equilibrium

$$K_{eq} = \frac{I_{FeSH^+} \times p_{HCl}}{I_{FeCl^+} \times p_{H_2S}} \qquad (2)$$

constant is estimated as 30%, comprising the experimental uncertainties as well as systematic errors.[25] Note that the considerable error in absolute pressure measurement[22] is not relevant here. Comparison of the measured $\Delta_r G_{298}$ to the 0 K reaction thresholds obtained with the GIB method requires conversion of $\Delta_r G_{298}$ to $\Delta_r H_0$ values by utilizing calculated entropies and thermal corrections (Table 1).

TABLE 1: Entropies and Thermal Corrections to Enthalpies for Selected Molecules at 298 K Calculated at the B3LYP/6-311+G* Level of Theory

	entropy [cal/(mol K)]	$\Delta(H_{298} - H_0)$ (kcal/mol)
HCl	44.6	6.2
H_2S	49.2	11.7
$FeCl^+$	59.4	2.9
$FeSH^+$	65.5	7.8

Calculations. All computations are performed on either IBM/RS 6000 workstations or a CRAY-YMP supercomputer. For the calculations of geometries and energetics, a density functional theory (DFT) approach is applied in which the B3LYP hybrid method[26] is combined with the 6-311+G* basis sets as implemented in the Gaussian94 program package.[27] The B3LYP approach has been shown to provide reasonably accurate energetics for small iron compounds.[28] Stationary points are characterized as minima or first-order transition states by evaluation of the frequencies and normal modes. The computed rotational constants and unscaled vibrational frequencies are also used for converting between 0 and 298 K data. The minima connected with the transition structures are characterized by internal reaction coordinate (IRC) calculations. Corrections for zero-point vibrational energy (ZPVE) are included, if not stated otherwise.

Experimental Results

First, we present the results of the ion−molecule reaction of FeS^+ with D_2 as studied with the GIB instrument. In these experiments, deuterium is used simply to reduce mass overlap due to the limited mass resolution of the quadrupole analyzer, while the FT-ICR studies as well as the theoretical treatment refer to the protio variants. Owing to the use of deuterium instead of hydrogen in the GIB experiment, the reaction thresholds differ slightly as compared to the unlabeled system. For comparison with the protio system, the calculated zero-point energies of the labeled and unlabeled species were considered, and both the thresholds for the $[Fe,D_2,S]^+$ and the ZPVE corrected thresholds for the $[Fe,H_2,S]^+$ system are given below. The bond-dissociation energy $D_0(Fe^+-SH)$ is evaluated by applying the bracketing technique and performing equilibrium measurements in the FT-ICR instrument. The presentation of the experimental results is followed by a discussion of the calculated potential-energy surface (PES) for the $[Fe,H_2,S]^+$ system, in which the different routes for H−H bond activation

TABLE 2: Heats of Formation and Dissociation Energies for Ionic and Neutral Species at 0 K[a]

species	$\Delta_f H_0$ (kcal/mol)	D_0 (kcal/mol)
H	51.6	
D	52.5	
S(g)	65.7 ± 0.1	
H_2	0	103.2 ± 0.0
D_2	0	105.0 ± 0.0
SH[b]	34.1 ± 0.7	83.2 ± 0.7
SD[b]	34.5 ± 0.7	83.7 ± 0.7
H−SH	−4.2 ± 0.2	89.9 ± 0.7
D−SD	−5.0 ± 0.2	92.0 ± 0.7
Cl	28.6 ± 0.0	
Br	28.2 ± 0.0	
OH	9.2 ± 0.3	
HCl	−22.0 ± 0.1	102.2 ± 0.1
HBr	−6.8 ± 0.1	86.6 ± 0.1
H−OH	−57.1 ± 0.0	117.9 ± 0.3
Fe^+	280.2 ± 1.8	
FeS^+[c]	274.5 ± 2.0	71.3 ± 0.9
FeH^+[d]	282.9 ± 2.3	48.9 ± 1.4
FeD^+[d]	282.7 ± 2.3	50.0 ± 1.4
Fe^+−SH[e]	248.3 ± 3.2	66.0 ± 2.6
$FeCl^+$[f]	229.2 ± 3.1	79.6 ± 2.5
$FeBr^+$[g]	232.3 ± 5.3	76.1 ± 5.0
Fe^+−OH[d]	201.9 ± 3.4	87.5 ± 2.9
FeO^+[d]	259.1 ± 2.2	80.1 ± 1.2

[a] Chase, M. W., Jr.; Davies, C. A.; Downey, J. R., Jr.; Frurip, D. J.; McDonald, R. A.; Syverud, A. N. *J. Phys. Chem. Ref. Data* **1985**, *14*, Suppl. 1 (JANAF Tables). [b] Reference 33. [c] Reference 31. [d] Reference 6c. [e] This work. [f] Reference 30. [g] Reference 20.

by FeS^+ are described in detail. We note in passing that by analogy to the related FeO^+/H_2 system,[22,29] tunneling phenomena are neglected.

GIB. The reaction of FeS^+ with D_2 yields Fe^+, FeD^+, and $FeSD^+$ as ionic products according to reactions 3−5. The product distribution resembles that detected in the reaction of

$$FeS^+ + D_2 \rightarrow \begin{cases} Fe^+ + D_2S - 0.03\ (0.06) \pm 0.06\ \text{eV} & (3a) \\ Fe^+ + D_2 + S - 3.09\ (3.09) \pm 0.04\ \text{eV} & (3b) \\ FeD^+ + SD - 1.85\ (1.84) \pm 0.08\ \text{eV} & (4a) \\ FeD^+ + S + D - 5.48\ (5.45) \pm 0.07\ \text{eV} & (4b) \\ FeSD^+ + D - 1.16\ (1.10) \pm 0.12\ \text{eV} & (5) \end{cases}$$

FeO^+ with molecular hydrogen (H_2, HD, and D_2), where the corresponding products Fe^+, FeH^+ (FeD^+), and $FeOH^+$ ($FeOD^+$) are observed.[29] The thermochemistry indicated in the equations is calculated using the 0 K values given in Table 2 and refers to the formation of the species in their ground states. The thermochemistry given in parentheses refers to the protio variant $FeS^+ + H_2$, which is needed further below for comparison with the FT-ICR data and the theoretical results.

The cross sections for all three ionic products are depicted in Figure 1. The least endothermic process observed is formation of Fe^+, reaction 3. The Fe^+ cross section exhibits a rather unusual shape. It rises from an apparent threshold of about 0.6 eV, increases more slowly between 1.3 and 1.8 eV but again more rapidly above 1.8 eV. Then, the Fe^+ cross section peaks at about 2.8 eV and rises again above 3.5 eV. Analysis of the threshold region using eq 1 yields $E_0 = 0.64 \pm 0.11$ eV (Table 3), i.e., ca. 0.6 eV above the thermochemical threshold of reaction 3a. This result implies that the measured threshold of the Fe^+ channel reflects a barrier in excess of the reaction endothermicity rather than the thermochemical threshold; we return to this aspect below. The change in slope at about 1.5 eV coincides with the appearance of the $FeSD^+$ product channel, pointing to a competition with the more efficient $FeSD^+$. The slight increase of $\sigma(Fe^+)$ that becomes obvious above 3.5 eV can be assigned to simple collision-induced dissociation (CID) of FeS^+, reaction 3b.

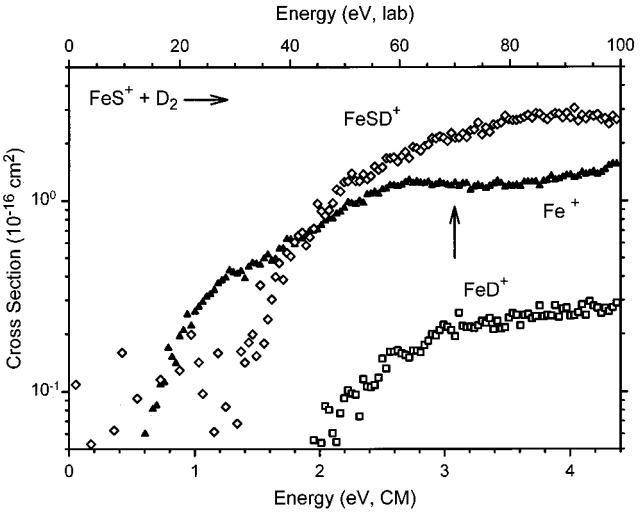

Figure 1. Product cross sections for the reaction of FeS^+ and D_2 to form Fe^+ (▲), FeD^+ (□), and $FeSD^+$ (◇) as a function of kinetic energy in the center-of-mass (lower axis) and laboratory (upper axis) frames. The arrow marks the Fe^+−S bond energy at 3.09 ± 0.04 eV.

TABLE 3: Summary of Parameters in Eq 1 Used for the Fits of the Cross Sections

reaction	E_0, eV[a]	σ_0	n
$FeS^+ + D_2 \rightarrow Fe^+ + D_2S$ (3)	0.64 ± 0.11	0.91 ± 0.30	1.29 ± 0.28
$FeS^+ + D_2 \rightarrow FeD^+ + DS$ (4)	1.82 ± 0.35	0.42 ± 0.20	1.16 ± 0.51
$FeS^+ + D_2 \rightarrow FeSD^+ + D$ (5)	1.52 ± 0.14	3.86 ± 0.35	1.19 ± 0.13

[a] The E_0 values are the average of several threshold fits with uncertainties of one standard deviation.

Formation of FeD^+ is the least efficient reaction channel. Occurrence of reaction 4b can be ruled out immediately due to its high thermodynamic threshold, which is beyond the range of energies studied. Thus, we assign the experimental threshold to reaction 4a. Analysis of the FeD^+ cross section with eq 1 yields $E_0 = 1.82 \pm 0.35$ eV (Table 3). This agrees well with the threshold of 1.85 ± 0.08 eV calculated from the literature thermochemistry (Table 2).[30] The difference between hydrogen and deuterium is small, as the contributions from H_2 and D_2 versus $FeH^+ + HS$ and $FeD^+ + DS$ cancel each other. For the protio variant, the threshold translates to $E_0 = 1.82 \pm 0.35$ eV.

The $FeSD^+$ channel rises from an apparent threshold of about 1.4 eV and peaks at about 4.0 eV. The formation of $FeSD^+$ is the most efficient channel observed above 2 eV. However, mass overlap with the close-lying parent-ion beam (FeS^+) causes a low signal/noise ratio in the data, especially at low interaction energies. Therefore, we cannot exclude a minor (cross section $< 10^{-17}$ cm^2), less endothermic contribution to the $FeSD^+$ channel (see below). Analysis of the apparent threshold region with eq 1 yields $E_0 = 1.52 \pm 0.14$ eV (Table 3), which would translate into $D_0(Fe^+-SD) = 57.6 \pm 3.4$ kcal/mol and $D_0(Fe^+-SH) = 56.9 \pm 3.4$ kcal/mol for the protio variant, respectively.

The FT-ICR bracketing results given below demonstrate that this value for $D_0(Fe^+-SH)$ is too small, indicating that the GIB experiment probes the presence of a reaction barrier rather than the asymptotic reaction endothermicity. In addition, some quite general thermochemical considerations support this conjecture. An Fe^+−SH bond energy of 56.9 ± 3.4 kcal/mol would be significantly smaller than $D_0(Fe^+-S) = 71.3 \pm 0.9$ kcal/mol.[31]

Exactly the opposite trend is observed for the $FeO^+/FeOH^+$ couple,[6c] where the bond strength of Fe^+-OH exceeds that of Fe^+-O by 7.4 kcal/mol. Further, the NH and NH_2 fragments, isoelectronic with O and OH, respectively, also show an increase in going from Fe^+-NH (69.0 ± 2.0 kcal/mol)[32] to Fe^+-NH_2 (73.9 ± 2.3 kcal/mol).[6c] Considering the general differences between second- and third-row elements, a slight decrease from $D_0(Fe^+-S)$ to $D_0(Fe^+-SH)$ may occur. For example, the differences[33] between the first and second bond strengths in the element hydrides (EH_n), i.e., $D_0(H_{n-1}E-H)$ and $D_0(H_{n-2}E^{\bullet}-H)$, amount to 16.8 kcal/mol for E = O ($n = 2$) and 10.9 kcal/mol for E = N ($n = 3$), compared to only 6.8 kcal/mol for E = S ($n = 2$). Overall, a decrease from $D_0(Fe^+-S) = 71.3 \pm 0.9$ kcal/mol to $D_0(Fe^+-SH) = 56.9 \pm 3.4$ kcal/mol is unexpected and thus indicates an anomalous trend for the iron/sulfur bonding.

FT-ICR. Ligand exchange is one obvious way to obtain upper and lower bounds for the Fe^+-SH bond strength. To this end, the ligand-exchange reactions $FeX^+ + H_2S \rightarrow FeSH^+ + XH$ (X = OH, Cl, and Br; reactions 6−8) were investigated with FT-ICR.

$$FeOH^+ + H_2S \rightarrow FeSH^+ + H_2O \quad (6)$$

$$FeCl^+ + H_2S \rightarrow FeSH^+ + HCl \quad (7)$$

$$FeBr^+ + H_2S \rightarrow FeSH^+ + HBr \quad (8)$$

Reaction 6 occurs with a moderate efficiency ($k/k_{capt} = 0.3$),[34] while the use of chlorine as a ligand, reaction 7, causes the reaction efficiency to drop by 1 order of magnitude ($k/k_{capt} = 0.03$). The exchange of the bromine ligand for SH, reaction 8, is not observed within the experimental accuracy ($k/k_{capt} < 0.0005$). Given the bond-dissociation energies of Fe^+-OH, Fe^+-Cl, and Fe^+-Br in Table 2,[20,29c,35] our results for reactions 6 and 8 provide a bracket of 59.5 ± 3.0 kcal/mol $\leq D_0(Fe^+-SH) \leq 79.4 \pm 5.0$ kcal/mol. Because of fortunate circumstances, $D_0(Fe^+-SH)$ can be further refined by consideration of process 7. The low reaction rate of (7) can be rationalized in two ways. Either the reaction is slightly endothermic or a significant, but surmountable, barrier is involved. This ambiguity can be resolved by conducting equilibrium measurements. To establish an equilibrium, $FeSH^+$ is trapped in ca. 1:2 and 1:1 mixtures of H_2S and HCl at different total pressures in the range of 5×10^{-9} to 2×10^{-8} mbar.[24]

The analysis of these experiments according to eq 2 yields an equilibrium constant $K_{eq} = 0.6 \pm 0.2$ and thus $\Delta_r G_{298} = 0.3 \pm 0.2$ kcal/mol. $\Delta_r G_{298}$ is converted into $\Delta_r H_{298} = 0.7 \pm 0.2$ kcal/mol using $\Delta_r S_{298} = 1.5$ cal/(mol K) derived from the entropies listed in Table 1. Further, $\Delta_r H_{298}$ is transformed to 0 K thermochemistry by use of the calculated enthalpy corrections, which leads to $\Delta_r H_0 = 1.3 \pm 0.2$ kcal/mol. Consequently, $D_0(Fe^+-SH) = 66.0 \pm 2.6$ kcal/mol, from which $\Delta_f H_0(FeSH^+) = 248.3 \pm 3.2$ kcal/mol is derived.

Combined with literature thermochemistry, this bond energy yields $\Delta_r H_0 = 25.3 \pm 2.8$ kcal/mol for reaction 5, which is in obvious disagreement with $E_0 = 1.49 \pm 0.14$ eV (34.4 ± 3.2 kcal/mol) as derived from GIB measurements with H/D correction. There are several ways to rationalize this discrepancy. One possibility is that different products are formed in the two experimental approaches, i.e., either $FeSH^+$ vs $HFeS^+$ isomers and/or different electronic states. However, if the same product is formed in the same state in both experiments, the only reasonable explanation would be the presence of a significant barrier in reaction 5.

SCHEME 1

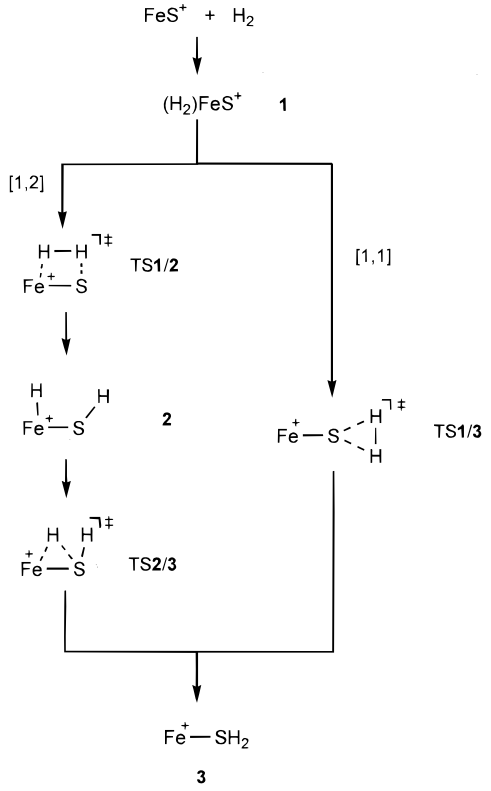

Theoretical Results

Clarification of the origin of the discrepancies between the FT-ICR and GIB results for $D_0(Fe^+-SH)$ can be achieved by consulting the calculated potential-energy surface for the $[Fe,H_2,S]^+$ system. Two conceivable mechanisms are considered for the reaction of FeS^+ with H_2 after formation of the encounter complex $(H_2)FeS^+$, **1** (Scheme 1).[29b,36] (i) Concerted [1,1]-addition of dihydrogen to the sulfur atom to form the $Fe(SH_2)^+$ product complex, **3**. (ii) [1,2]-Addition across the Fe−S bond leading initially to the insertion intermediate $HFeSH^+$, **2**, which subsequently proceeds to $Fe(SH_2)^+$ via hydrogen migration (**2** → TS**2**/**3** → **3**). In the next sections, the structures, symmetries, and electronic states of all stationary points are presented (Charts 1 and 2) followed by a discussion of the two mechanisms. The error of the calculations is estimated to be ± 6.0 kcal/mol.[37]

Reactants. In agreement with earlier results,[10g,38] the ground state of FeS^+ is calculated to be a $^6\Sigma^+$ state with a $^4\Pi$ state 5.5 kcal/mol higher in energy. The $^6\Sigma^+$ state is represented by a $1\sigma^2 2\sigma^2 1\pi^4 1\delta^2 2\pi^2 3\sigma^1$ occupation of the valence orbitals in a one-configuration picture.[29d,39] B3LYP/6-311+G* predicts the r_{Fe-S} bond lengths as 2.06 Å ($^6\Sigma^+$) and 2.11 Å ($^4\Pi$), respectively. H_2 has a $^1\Sigma_g^+$ ground state with a bond length (r_{H-H}) of 0.74 Å. In the following, all calculated energetics will be given with respect to the FeS^+ ($^6\Sigma^+$) + H_2 ($^1\Sigma_g^+$) asymptote ($E_{rel} = 0$ kcal/mol), if not stated otherwise.

Minima. Three sets of minima are located for the $[Fe,H_2,S]^+$ system starting from $FeS^+ + H_2$. The first minimum (Chart 1) is the encounter complex **1** ($^6A_1$) located on the sextet surface with a planar C_{2v} geometry where the intact H_2 molecule ($r_{H-H} = 0.77$ Å) approaches the iron atom. This coordination seems reasonable as most of the charge in the FeS^+ cation is localized at the iron center (+0.64) and the bonding interaction in the encounter complex is determined by ion/induced-dipole forces. Accordingly, **1** ($^6A_1$) is only 8.9 kcal/mol below the entrance channel. The quartet minimum **1** ($^4A'$) is not perfectly planar

CHART 1

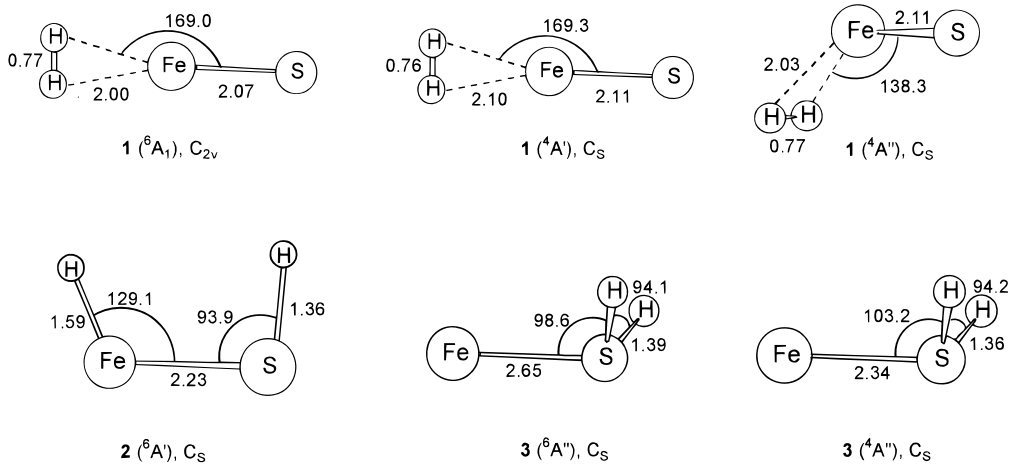

CHART 2

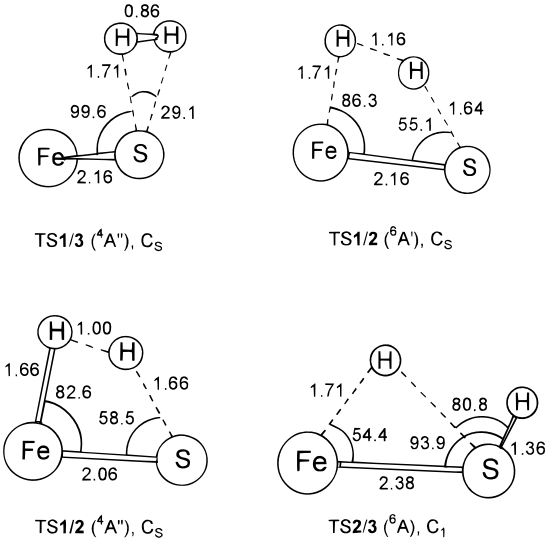

(C_s symmetry) and is located 5.5 kcal/mol above the corresponding sextet ground state **1** ($^6A_1$). A second bent structure **1** ($^4A''$) with the H_2 approaching the iron atom from the side of the FeS^+ molecule, thereby forming a dihedral HHFeS angle of 102°, lies only 0.3 kcal/mol above the $^4A'$ state. The small energy separation of **1** ($^4A'$) and **1** ($^4A''$) prevents a definitive assignment of the quartet ground state and further implies that the quartet surface is quite flat with respect to the rotation of the H_2 unit around the iron atom.

The next minimum on the sextet surface is the [1,2]-addition product, **2** ($^6A'$). It has a planar structure with a considerably elongated FeS bond as compared to **1** ($^6A_1$) and free FeS^+ (2.23 vs 2.07 and 2.06 Å, respectively). The rationale for the bond lengthening is the formation of the two bonds to hydrogen, which causes a reduction of the Fe−S bond order. No comparable minimum structure is found on the quartet surface (see below). The third type of minima are the C_s symmetric $Fe(SH_2)^+$ complexes **3** ($^4A''$) and **3** ($^6A''$). The geometries of the H_2S moieties in these two complexes are similar to each other and resemble that of free H_2S (1.35 Å, 93°). The Fe−S bond length is of particular interest, in that the quartet state has a much closer contact than the sextet (2.34 vs 2.65 Å). In addition, a planar $Fe(SH_2)^+$, **3** ($^6B_2$), complex with C_{2v} symmetry (not shown) is located 8.9 kcal/mol above the $^6A''$ state. While one might intuitively expect the H_2S dipole to be aligned with the positive charge on Fe^+, the existence of similar bent minima have previously been reported for $M(H_2O)^+$ and $M(H_2S)^+$ complexes and were traced back to the balance between electrostatic and covalent bonding in the bent structures.[40,41]

Transition Structures. The [1,1]-addition mechanism proceeds via a single transition structure, denoted as TS**1**/**3** (Chart 2), en route to the formation of the $Fe(SH_2)^+$ complex **3**. Conceptually, the [1,1]-route in the FeS^+/H_2 system corresponds to the "oxene-pathway" proposed in the chemistry of transition-metal oxenoids.[42] Thus, interconversion of **1** into **3** requires reorientation of the complexed hydrogen molecule from the iron to sulfur prior to passage via TS**1**/**3**. The IRC calculations confirm that no additional mimina are involved in the sequence **1** → TS**1**/**3** → **3**. The transition structure located on the quartet surface at E_{rel} = 18.6 kcal/mol has C_s symmetry ($^4A''$) and is characterized by a somewhat elongated H−H bond (0.86 vs 0.77 Å) concomitant with two S−H bonds that are longer than those found in free H_2S (1.71 vs 1.35 Å). The imaginary frequency (i1256 cm^{-1}) of TS**1**/**3** ($^4A''$) corresponds to the movement of the two hydrogen atoms toward the sulfur atom under elongation of the H−H bond. Location of an equivalent sextet TS**1**/**3** is not further pursued, because vertical excitation to the sextet surface at the optimized geometry of TS**1**/**3** ($^4A''$) led to a splitting of 74.1 kcal/mol. This huge energy demand leads us to exclude the [1,1]-route on the sextet surface from further consideration. Note that the assumption of similar geometries for sextet and quartet species is justified by comparison to the geometric parameters of other stationary points (Charts 1 and 2).

The [1,2]-addition mechanism involves two consecutive steps. The reaction commences with an addition of H_2 across the FeS^+ unit, **1** → **2**, followed by a [1,2]-hydrogen shift from iron to sulfur, **2** → **3**. The transition structure TS**1**/**2** ($^6A'$) for the [1,2]-addition (E_{rel} = 17.9 kcal/mol) comprises a planar, four-membered ring in which the H−H bond (1.16 Å) is already much longer than that of an intact H_2 molecule (0.74 Å) and the Fe−H bond is close to that of **2** ($^6A'$) (1.71 vs 1.59 Å), while the S−H interaction is still weak (1.64 vs 1.36 Å). The imaginary frequency (i1603 cm^{-1}) is assigned to the stretch of the H_2 moiety with simultaneous movement of the H atoms toward iron and sulfur. The corresponding quartet species TS**1**/**2** ($^4A''$) with E_{rel} = 12.8 kcal/mol shows a structure close to TS**1**/**2** ($^6A'$), but with shorter H−H, Fe−H, and Fe−S bond lengths; the largest difference of 0.16 Å is found for the H−H distance. In the quartet TS, the imaginary frequency can be attributed to the same motion as for the sextet, although the frequency itself is about 30% lower (i1096 cm^{-1}). Qualitatively, the Fe−S and

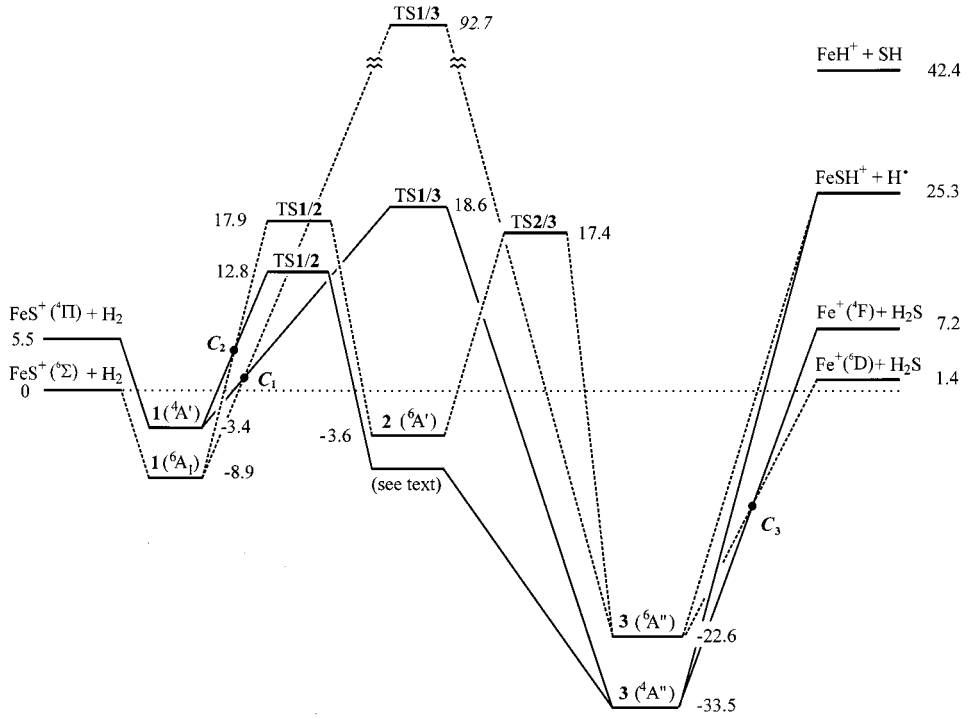

Figure 2. Potential-energy surface of the reaction $FeS^+ + H_2$. Energies (in kcal/mol) are given relative to the FeS^+ ($^6\Sigma^+$) + H_2 ($^1\Sigma^+$) with ZPVE correction included. The dashed lines correspond to the sextet surface, while the solid lines denote the quartet PES. The thermochemistry given for the product channels corresponds to experimental data; see text for discussion. C_1-C_3 denote the tentative crossing points between the sextet and quartet surfaces discussed in the text.

H−H bonds are more reactant-like in the quartet TS than in the sextet and hence it is an earlier TS than on the sextet surface.

The subsequent [1,2]-hydrogen shift from iron to sulfur to form $Fe(SH_2)^+$ can occur via the C_1-symmetrical TS**2**/**3** (^{6}A) with E_{rel} = 17.4 kcal/mol. In TS**2**/**3** (^{6}A), the Fe−H bond is lengthened and the hydrogen atom is located approximately above the middle of the Fe−S bond (Chart 2). The imaginary frequency (i1107 cm^{-1}) can be assigned to the motion of the hydrogen atom from iron to sulfur. In accord with the 1,2-hydrogen shift, a lengthening of the Fe−S bond by 0.15 Å is observed between **2** (^{6}A′) and TS**2**/**3** (^{6}A). Attempts to locate a similar TS on the quartet surface failed (see below).

Products. Experimentally, Fe^+, FeD^+, and $FeSD^+$ are observed as ionic products in the reaction of FeS^+ with D_2, processes 3−5, Table 3. After considering H and D variants, the thresholds of these reactions for the corresponding protio species are 15.8 ± 2.5, 42.0 ± 8.1, and 34.4 ± 3.2 kcal/mol, respectively, as compared to the thermochemical reaction enthalpies of 1.4 ± 1.3, 42.4 ± 1.8, and 25.3 ± 2.8 kcal/mol (Table 2). At the B3LYP/6-311+G* level of theory, the ground state of Fe^+ is predicted to be Fe^+ (^{4}F), being 5.0 kcal/mol more stable than the ^{6}D state. A reversed order is found experimentally with the Fe^+ (^{6}D) ground state located 5.8 kcal/mol below the ^{4}F state.[43] The failure to properly describe the energetics of spin states can be attributed to a bias toward $3d^n$ configurations over $3d^{n-1}4s^1$ configurations almost inherent to the description of atomic transition-metal ions in DFT methods.[28,44] Therefore, the calculation of the bare Fe^+ ion is associated with a larger error than the other parts of the PES. To account for this in the PES, we use the experimental state splitting between the ^{6}D and ^{4}F states; however, the energies of no other species are adjusted.[45]

For $[Fe,S,H]^+$, two different connectivities, $SFeH^+$ and $FeSH^+$, are conceivable. The formation of ground-state $FeSH^+$ (^{5}A′) is calculated to be endothermic by 25.2 kcal/mol. This value is in excellent agreement with $\Delta_r H_0$ = 25.3 ± 2.8 kcal/mol calculated for the protiated version of reaction 5 using D_0[Fe^+−SH] from the FT-ICR experiments. $FeSH^+$ (^{5}A′) has C_s symmetry with an FeSH angle of 94°, r_{Fe-S} = 2.17 Å, and r_{S-H} = 1.36 Å. Another bent quintet structure (^{5}A″) with an FeSH angle of 110° is located 18.0 kcal/mol above the ^{5}A′ ground state. Excitations to the lowest triplet (^{3}A′) and septet (^{7}A′) states require 17.9 and 43.8 kcal/mol, respectively. The lowest electronic state of the second structural isomer, $SFeH^+$ (^{3}A′), is calculated to lie 45.7 kcal/mol higher in energy than the ^{5}A′ ground state of $FeSH^+$ and is therefore excluded from further consideration.

Formation of the third reaction product, FeH^+, is calculated to be endothermic by 36.5 kcal/mol, in agreement with the literature thermochemistry of 42.4 kcal/mol calculated for the protiated version of reaction 4. The ground state of FeH^+ is a quintet ($^5\Delta$),[46] while the lowest triplet state ($^3\Pi$)[47] lies 32 kcal/mol higher in energy at the B3LYP/6-311+G* level.

When the calculated stationary points are combined, the potential-energy surface depicted in Figure 2 is obtained. Energies for the product channels are adopted from the literature data given in Table 2. In the following section, the [1,1]- and [1,2]-addition mechanisms will be discussed with respect to the quartet and sextet surfaces.

Discussion

Starting from the ground-state entrance channel, FeS^+ ($^6\Sigma^+$) + H_2, and the encounter complexes (**1**, Chart 1), the reaction can proceed by at least two different pathways.[48]

[1,1]-Addition. The occurrence of [1,1]-addition entirely on the sextet surface is excluded from further consideration due to the high barrier associated with TS**1**/**3** (see above). Instead, the system may cross from the sextet to the quartet surface at the putative crossing point C_1 situated between **1** ($^6A_1$) and TS**1**/**3** (^{4}A″). The relevance of such crossings in oxidations and the requirements for violation of spin conservation have been

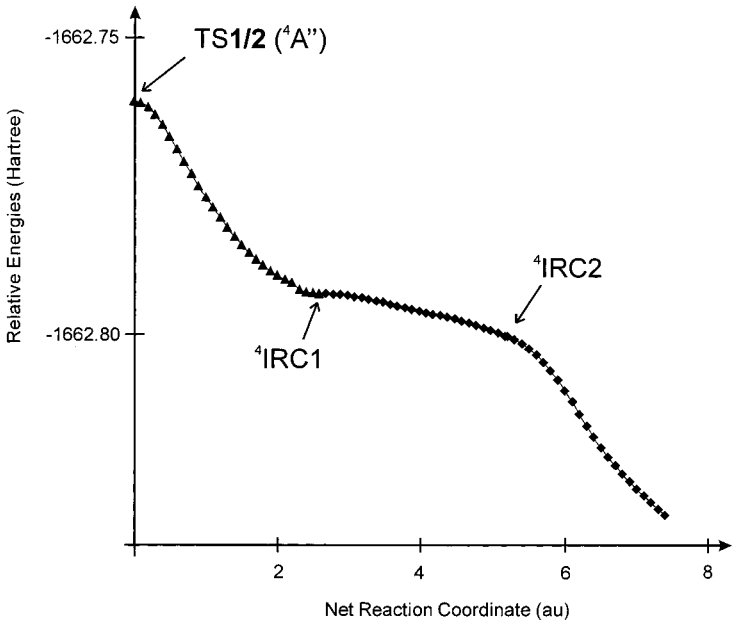

Figure 3. IRC calculation from TS**1**/**2** (^{4}A″) to $Fe(SH_2)^+$, **3** (^{4}A″). Energies are given in hartrees without ZPVE correction. Note that the calculation applied "normal" convergence criteria between TS**1**/**2** (^{4}A″) and the structure ^{4}IRC1, while "tight" convergence criteria were used afterward (see text).

discussed in detail previously.[29,36,39,49] As verified by IRC calculations, the system proceeds from TS**1**/**3** (^{4}A″) to the global minimum **3** (^{4}A″). The $FeSH^+$ (^{5}A′) + H and Fe^+ (^{4}F) + H_2S product channels can be accessed from **3** (^{4}A″) without further structural rearrangements, while the formation of Fe^+ (^{6}D) + H_2S requires a second surface crossing back to the sextet surface at C_3. In summary, the $FeS^+ + H_2$ reaction can progress via a [1,1]-addition, but this involves a surface crossing and a barrier. Considering the estimated uncertainty of ±6 kcal/mol in the calculations, the predicted barrier height (E_{rel} = 18.6 kcal/mol) is somewhat higher but within the error margin of the experimental threshold of 15.8 ± 2.5 kcal/mol for the formation of Fe^+. Note that the predicted barrier is far below the thermochemical threshold for formation of $FeSH^+$. Further, the [1,1]-addition mechanism does not give an explanation for the apparent barrier in the $FeSH^+$ channel, and formation of FeH^+ is not directly accessed via the [1,1]-route, which implies that the [1,2]-pathway must contribute to the observed reactivity.

[1,2]-Addition. The respective sextet and quartet surfaces are discussed separately for the [1,2]-addition sequence because the two surfaces differ dramatically.

On the sextet surface, the [1,2]-addition proceeds from the encounter complex **1** via TS**1**/**2** (^{6}A′) to minimum **2** (^{6}A′), as revealed by IRC calculations. The insertion intermediate **2** (^{6}A′) has three options for further reaction. It can either (i) decompose to the reactants, (ii) undergo a second hydrogen shift via TS**2**/**3** (^{6}A), or (iii) directly dissociate into the FeH^+ + HS and $FeSH^+$ + H fragments. Once the energy is available, the dissociations are expected to be favored and should lead to formations of FeH^+ and $FeSH^+$ at their thermodynamic thresholds. Note, that this is again in disagreement with the experimentally observed barrier for $FeSH^+$ formation. Processes (i) and (ii) have similar barriers, with TS**2**/**3** (^{6}A) being a little lower, shifting the reaction toward **3** (^{6}A″). As soon as **3** (^{6}A″) is reached, formation of ground-state $FeSH^+$ and Fe^+ is conceivable without further structural rearrangement. Note that both barriers for formation of Fe^+ on the sextet surface (17.9 and 17.4 kcal/mol) are somewhat higher than the experimentally observed threshold (15.8 ± 2.5 kcal/mol) but still within experimental error.

CHART 3

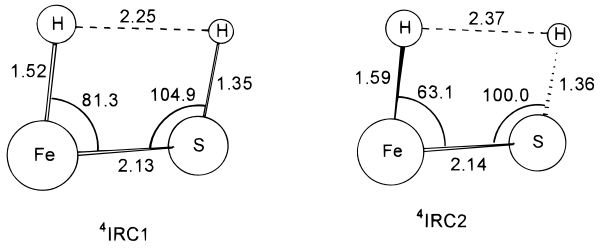

On the quartet surface, the [1,2]-addition very much resembles the situation found for the sextets at structures **1**, **3**, and TS**1**/**2**. However, the quartet and sextet surfaces differ entirely between TS**1**/**2** and **3**. While the inserted structure **2** (^{6}A′) and the related transition structure TS**2**/**3** (^{6}A) exist as stationary points on the sextet surface, neither of the corresponding quartet species can be located. Instead, tedious IRC calculations starting from TS**1**/**2** (^{4}A″) lead to the picture shown in Figure 3. Following the imaginary modes of TS**1**/**2** (^{4}A″), the H−H distance elongates while the Fe−H and S−H bonds shorten. Simultaneously, the HSFe and SFeH angles increase until a stationary point ^{4}IRC1 is indicated by IRC calculations using the "normal" convergence criteria.[50] The structure of the planar ^{4}IRC1 (Chart 3) is comparable to that of **2** (^{6}A′) but cannot be assigned to the quartet insertion intermediate, as a frequency calculation on this structure yields a sizable imaginary frequency (i357.6 cm^{-1}). The latter corresponds to an out-of-the-plane rotation of the two hydrogen atoms, viz. a rotation around the Fe−S bond. Therefore, structure ^{4}IRC1 for which the B3LYP calculation terminates the IRC at "normal" convergence criteria cannot be regarded as a stationary point, but a spurious minimum. In fact, when the IRC calculation is restarted at the geometry of ^{4}IRC1 while applying "tight" convergence criteria,[50] the system further proceeds to lower energies, though the potential is much flatter. The associated movement is best described as an increase of the dihedral HFeSH angle concomitant with a slight elongation of the Fe−S bond. At a dihedral angle of about 80°, the mode for the out-of-the-plane rotation has almost deceased (sketched as structure ^{4}IRC2) and a new mode corresponding to the 1,2-

hydrogen shift from Fe toward S begins to contribute to the reaction coordinate. Following the new mode the energy decreases more rapidly, and the IRC calculation terminates at a structure close to that of minimum **3** (^{4}A″).

A similar phenomenon was found by Tilson and Harrison,[51] who reported calculations on the reaction of scandium sulfide cation with dihydrogen, where the inserted structure also does not correspond to a true minimum but rather to a saddle point from which the energy further decreases by rotation of the hydrogen atoms out of the plane of the molecule. It may be possible to further resolve the shape of the "plateau" between ^{4}IRC1 and ^{4}IRC2 by use of different methods and basis sets. This is deemed unnecessary, however, as any barrier associated with this TS would still be very small, leading to similar conclusions and arguments as presented below. The IRC calculation depicted in Figure 3 reveals that the region between ^{4}IRC1 and ^{4}IRC2 is rather flat (within 5 kcal/mol). Thus for the reaction under study, which is examined at thermal conditions (298 K), we may safely neglect any minima in this region but rather treat the putative insertion structure ^{4}IRC1 as a contributing dimension to the density of states of excited **3** (^{4}A″). Overall, this implies that once the FeS^+/H_2 couple has enough energy to overcome the barrier associated with TS**1**/**2** (^{4}A″) (E_{rel} = 12.8 kcal/mol), it continues through ^{4}IRC1 and ^{4}IRC2 to the product complex **3** (^{4}A″). Note that TS**1**/**2** (^{4}A″) has the lowest energy demand of all TS considered for the $[Fe,H_2,S]^+$ system and falls within the error margins of the experimentally observed threshold for $Fe^+ + H_2S$ formation. From **3** (^{4}A″), the Fe^+ (^{4}F) and $FeSH^+$ (^{5}A′) channels can be accessed directly, while formation of ground-state Fe^+ (^{6}D) requires a surface crossing from the quartet back to the sextet surface at C_3. Compared to the sextet surface, the FeH^+ channel is less likely to be accessed from the quartet surface, due to the absence of a distinct minimum for structure **2**.

In summarizing the mechanistic details, we arrive at the following picture: (i) formation of ground-state Fe^+ (^{6}D) is most likely to proceed via the [1,2]-addition mechanism with two surface crossings at C_2 and C_3 leading to a computational prediction of an activation barrier having $E_{rel} = 12.8 \pm 6.0$ kcal/mol, which is in reasonable agreement with the threshold $E_0 = 15.8 \pm 2.5$ kcal/mol measured for reaction 3a. Note, however, that formation of excited Fe^+ (^{4}F) is also feasible, as it does not require a second spin crossing at C_3 and is energetically accessible at all energies above the measured activation barrier. (ii) None of the calculated barriers gives a reasonable explanation for the formation of $FeSH^+$ with an apparent threshold of $E_0 = 34.4 \pm 3.2$ kcal/mol. This is particularly surprising because reaction 5 can be described as a simple hydrogen atom abstraction from H_2 by the FeS^+ unit, a process that is not expected to show a very large barrier in excess of reaction endothermicity (see below). Thus, a more profound consideration of the entire PES is needed.

Direct access of the $FeSH^+ + H$ exit channel is conceivable from **2** (^{6}A′), **3** (^{6}A″), and **3** (^{4}A″). Starting from **3**, however, thermochemistry predicts the formation of $FeSH^+$ to be 23.9 ± 3.1 kcal/mol energetically disfavored compared to the $Fe^+ + H_2S$ channel, which is also accessible from **3**. This fact is likely to result in a strong competition between the two channels, with the $FeSH^+$ channel being disfavored. Such competition could cause a delayed threshold for the $FeSH^+$ channel. However, **2** (^{6}A′) should allow efficient formation of $FeSH^+$ because no competition with the Fe^+ channel is expected. This is because hydrogen migration to form **3** (^{6}A″) is associated with the significant barrier TS**2**/**3** (^{6}A), which renders the Fe^+ channel only 7.9 kcal/mol energetically more favorable than formation of $FeSH^+$, in contrast to the situation on the quartet surface. Nevertheless, there are two reasons why **2** (^{6}A′) has only a low probability to be formed. First, the predicted energetic position of TS**1**/**2** (^{6}A′) at E_{rel} = 17.9 kcal/mol does not allow for formation of **2** (^{6}A′) below this energy. Second, if we assume an efficient crossing between the sextet and quartet surfaces at C_2 most of the sextet species will flip spin and cross to the quartet surface. The efficiency of the crossing at C_2 appears to be sufficient to allow for reasonably intense formation of Fe^+ as soon as the interaction energy exceeds the barrier of TS**1**/**2** (^{4}A″). The probability for the reactant complex to traverse TS**1**/**2** (^{6}A′) at the calculated energy of E_{rel} = 17.9 kcal/mol is strongly reduced because of the lower energy demand of TS**1**/**2** (^{4}A″), for which the calculations predict E_{rel} = 12.8 kcal/mol. Hence, only a small percentage of reactant collisions will reach intermediate **2** (^{6}A′) at low interaction energies, while at higher interaction energies the crossing probability decreases as the motion of the reactants speeds up. Thus, more particles traverse TS**1**/**2** (^{6}A′) and access **2** (^{6}A′), where they primarily continue to form $FeSH^+$. Here, again, we expect a delayed threshold for the formation of $FeSH^+$ due to the competition between TS**1**/**2** (^{4}A″) and TS**1**/**2** (^{6}A′).

To summarize, the late threshold for the formation of $FeSH^+$, i.e., 34.4 ± 3.2 kcal/mol in the H/D corrected GIB experiment as compared to the literature value of 25.3 ± 2.8 kcal/mol, is attributed to the joint action of two related phenomena: (i) The nonexistence of the insertion structure on the quartet surface prompts the reaction to continue to form **3** (^{4}A″). Here, competition between the $Fe^+ + H_2S$ and $FeSH^+ + H$ exit channels discriminates against the latter channel by 23.9 kcal/mol, which results in a delayed formation of $FeSH^+$. (ii) The competition between TS**1**/**2** (^{4}A″) and TS**1**/**2** (^{6}A′) hinders the access to **2** (^{6}A′) and therefore delays the formation of $FeSH^+$ on the sextet surface. Finally, it is conceivable that loss of atomic hydrogen from the intermediates **1**−**3** (either quartet or sextet) is hindered by a potential-energy barrier in excess of reaction endothermicity, in contradiction to our assumptions made above. Such a scenario would provide an alternative explanation for the delayed appearance of the $FeSH^+$ channel. For the time being, we cannot treat this aspect comprehensively, however, recent theoretical studies of the related $[Fe,O,H_2]^+$ system[36,52] gave no indications for the presence of such barriers associated with hydrogen-atom loss.

Conclusions

In the seemingly simple reaction of FeS^+ with dihydrogen, only the high-energy channel leading to FeH^+ appears at thermodynamic threshold, while hydrodesulfurization to yield Fe^+ is affected by barriers and the explanation of the threshold for formation of $FeSH^+$ also requires consideration of the competing Fe^+ channel. The differences between experimental and calculated data are resolved by an inspection of the potential-energy surface, thereby explaining the product branching as a consequence of competing processes. In addition, $D_0(Fe^+-SH) = 66.0 \pm 2.6$ kcal/mol is derived from FT-ICR equilibrium measurements and is used to establish the thermochemistry of $FeSH^+$ formation from FeS^+ and H_2, $\Delta_r H_0 = 25.3 \pm 2.8$ kcal/mol.

The results are in line with a two-step [1,2]-addition mechanism that involves a change of spin multiplicity from the sextet surface of the reactants to the quartet surface for the intermediates. Specifically, the formation of the $FeD^+ + SD$ product channel agrees well between literature thermochemistry (1.85

± 0.08 eV) and GIB experiments (1.82 ± 0.35 eV). The threshold for $Fe^+ + D_2S$ formation in the GIB of 0.64 ± 0.11 eV (14.8 ± 2.5 kcal/mol) can be rationalized by the theoretically predicted barriers on both sextet and quartet surfaces (see Figure 2). In contrast, the delayed threshold of $FeSD^+$ formation in the GIB experiment cannot be explained by involving the minima and barriers alone but rather requires consideration of the competition between both the low-lying fragmentation channels and the spin crossing to the quartet surface versus adiabatic reaction on the sextet surface.

As far as the calculations are concerned, the agreement between theory and experiment is reasonable in most instances; however, some notorious cases remain, e.g., the splitting between the ^4F and ^6D states of Fe^+. From a chemical point of view, the performance of the B3LYP approach applied here is quite promising, because this reasonably economic level of theory provides valuable insight into the course of reactions involving transition metals.[10k,28,29d,35b,36,44,52] This is a formidable challenge that is rather difficult to treat comprehensively with other, more sophisticated methods using conventional ab initio theory.

Acknowledgment. This research was supported by the Deutsche Forschungsgemeinschaft, the Volkswagen-Stiftung, the Fonds der Chemischen Industrie (scholarship for I.K.), and the National Science Foundation (P.B.A.), CHE-9530412. We thank the Konrad-Zuse Zentrum Berlin for the generous allocation of computing time.

References and Notes

(1) Stiefel, E. I., Matsumoto, K., Eds. *Transition Metal Sulfur Chemistry*; ACS Symposium Series 653; American Chemical Society: Washington, DC, 1996.

(2) (a) Rodriguez, J. A.; Kuhn, M.; Hrbek, J. *J. Chem. Phys. Lett.* **1996**, *251*, 13. (b) Rodriguez, J. A.; Kuhn, M.; Hrbek, J. *J. Phys. Chem.* **1996**, *100*, 15494.

(3) (a) Takakuwa, S. In *Organic Sulfur Chemistry, Biochemical Aspects*; Oae, S., Okyama, T., Eds.; CRC Press: Boca Raton, FL, 1992; p 1 (b) Alpers, Ch. N., Blowes, D. W., Eds. *Environmental Geochemistry of Sulfide Oxidation*; ACS Symposium Series 550; American Chemical Society: Washington, DC, 1994.

(4) (a) Kaim, W.; Schwederski, B. *Bioanorganische Chemie*; Teubner: Stuttgart 1991. (b) Lippert, S. J.; Berg, J. M. *Principles of Bioinorganic Chemistry*; University Science Books: Mill Valley, CA, 1994.

(5) (a) Aliverti, A.; Piubelli, L.; Corrado, M.; Pandini, V. E.; Bellintani, F.; Curti, B.; Zanetti, G. In *Perspectives on Protein Engineering and Complementary Technologies*; Geisow, M., Epton, R., Eds.; Mayflower: Birmingham, U.K., 1995. (b) Millar, M.; Lee, J. F.; O'Sullivan, T.; Koch, S. A.; Fikar, R. *Inorg. Chim. Acta* **1996**, 243. (c) Trieber, C. A.; Rothery, R. A.; Weiner, J. H. *J. Biol. Chem.* **1996**, *271*, 4620. (d) Holm, R. H.; Kennepohl, P.; Solomon, E. I. *Chem. Rev.* **1996**, *96*, 2239. (e) Flint, D. H.; Allen, R. M. *Chem. Rev.* **1996**, *96*, 2315. (f) Beinert, H.; Kennedy, M. C.; Stout, C. D. *Chem. Rev.* **1996**, *96*, 2335. (g) Stephens, P. J.; Jollie, D. R.; Warshel, A. *Chem. Rev.* **1996**, *96*, 2491. (h) Que, L., Jr.; Ho, R. Y. N. *Chem. Rev.* **1996**, *96*, 2607. (i) Magalon, A.; Rothery, R. A.; Giordano, G.; Blasco, F.; Weiner, J. H. *J. Bacteriol.* **1997**, *179*, 5037. (j) Kaasjager, V. E.; Henderson, R. K.; Bouwman, E.; Lutz, M.; Spek, A. L.; Reedijk, J. *Angew. Chem., Int. Ed. Engl.* **1998**, *37*, 1668.

(6) (a) Eller, K.; Schwarz, H. *Chem. Rev.* **1991**, *91*, 1121. (b) Freiser, B. S. *J. Mass. Spectrom.* **1996**, *31*, 703. (c) Armentrout, P. B.; Kickel, B. L. In *Organometallic Ion Chemistry*; Freiser, B. S., Ed.; Kluwer: Dordrecht, The Netherlands, 1996.

(7) Fisher, E. R.; Elkind, J. L.; Clemmer, D. E.; Georgiadis, R.; Loh, S. K.; Aristov, N.; Sunderlin, L. S.; Armentrout, P. B. *J. Chem. Phys.* **1990**, *93*, 2676.

(8) Schröder, D.; Schwarz, H. *Angew. Chem., Int. Ed. Engl.* **1995**, *34*, 1973, and references therein.

(9) (a) Harris, S. *Chem. Phys.* **1982**, *67*, 229. (b) Harris, S.; Chianelli, R. R. *Chem. Phys. Lett.* **1983**, *101*, 603. (c) Bauschlicher, C. W.; Maitre, P. *Theor. Chim. Acta* **1995**, *90*, 189.

(10) (a) Müller, A.; Diemann, E.; Jostes, R.; Bögge, H. *Angew. Chem.* **1981**, *93*, 957. (b) Carlin, T. J.; Wise, M. B.; Freiser, B. S. *Inorg. Chem.* **1981**, *20*, 2745. (c) Jackson, T. C.; Carlin, T. J.; Freiser, B. S. *Int. J. Mass Spectrom. Ion Processes* **1986**, *72*, 169. (d) McMahon, T. J.; Jackson, T. C.; Freiser, B. S. *J. Am. Chem. Soc.* **1989**, *111*, 421. (e) Dance, I. G.; Fisher, K. J.; Willett, G. D. *Angew. Chem., Int. Ed. Engl.* **1995**, *34*, 201. (f) Dance, I. G.; Fisher, K. J.; Willett, G. D. *Inorg. Chem.* **1996**, *35*, 4177. (g) Harvey, J. N.; Heinemann, C.; Fiedler, A.; Schröder, D.; Schwarz, H. *Chem. Eur. J.* **1996**, *2*, 1230. (h) Kretzschmar, I.; Fiedler, A.; Harvey, J. N.; Schröder, D.; Schwarz, H. *J. Phys. Chem. A* **1997**, *101*, 6252. (i) Kretzschmar, I.; Schröder, D.; Schwarz, H. *Int. J. Mass Spectrom. Ion Processes* **1997**, *167/168*, 103. (j) Fisher, K.; Dance, I.; Willett, G. *J. Chem. Soc., Dalton Trans.* **1998**, 975. (k) Kretzschmar, I.; Schröder, D.; Schwarz, H.; Rue, C.; Armentrout, P. B. *J. Phys. Chem. A* **1998**, *102*, 10060.

(11) For metal−sulfide clusters, see, for example: (a) Ramli, E.; Rauchfuss, T. B.; Stern, C. L. *J. Am. Chem. Soc.* **1990**, *112*, 4043. (b) Nakat, J. H. E.; Dance, I. G.; Fisher, K. J.; Rice, D.; Willett, G. D. *J. Am. Chem. Soc.* **1991**, *113*, 5141. (c) Dehen, S.; Schäfer, A.; Ahlrichs, R.; Fenske, D. *Chem. Eur. J.* **1996**, *2*, 429. (d) Fisher, K.; Dance, I.; Willett, G.; Yi, M. *J. Chem. Soc., Dalton Trans.* **1996**, 709. (e) Nakajima, A.; Hayase, T.; Hayakawa, F.; Kaya, K. *Chem. Phys. Lett.* **1997**, *280*, 381. (f) Harvey, J. N.; Schröder, D.; Schwarz, H. *Inorg. Chim. Acta* **1998**, *273*, 111.

(12) (a) Ervin, K. M.; Armentrout, P. B. *J. Chem. Phys.* **1985**, *83*, 166. (b) Schultz, R. H.; Armentrout, P. B. *Int. J. Mass Spectrom. Ion Processes* **1991**, *107*, 29. (c) Schultz, R. H.; Crellin, K. C.; Armentrout, P. B. *J. Am. Chem. Soc.* **1991**, *113*, 8590. (d) Armentrout, P. B. In *Advances in Gas-Phase Ion Chemistry*; Adams, N. G., Babcock, L. M., Eds.; JAI Press: Greenwich, CT, 1992; Vol. 1, p 83.

(13) Beyer, T.; Swinehart, D. F. *Comm. Assoc. Comput. Machines* **1973**, *16*, 379.

(14) Herzberg, G. *Molecular Spectra and Molecular Structure*, reprint edition; Krieger: Malabar, FL, 1989 (Vol. I) and 1991 (Vol. III).

(15) Sunderlin, L. S.; Armentrout, P. B. *Int. J. Mass Spectrom. Ion Processes* **1989**, *94*, 149.

(16) (a) Dalleska, N. F.; Honma, K.; Armentrout, P. B. *J. Am. Chem. Soc.* **1993**, *115*, 12125. (b) Khan, F. A.; Clemmer, D. C.; Schultz, R. H.; Armentrout, P. B. *J. Phys. Chem.* **1993**, *97*, 7978. (c) Dalleska, N. F.; Honma, K.; Sunderlin, L. S.; Armentrout, P. B. *J. Am. Chem. Soc.* **1994**, *116*, 3519.

(17) Rodgers, M. T.; Armentrout, P. B. *J. Phys. Chem. A* **1997**, *101*, 2614.

(18) (a) Eller, K.; Schwarz, H. *Int. J. Mass Spectrom. Ion Processes* **1989**, *93*, 243. (b) Eller, K.; Zummack, W.; Schwarz, H. *J. Am. Chem. Soc.* **1990**, *112*, 621.

(19) Front-end resolution enhancement with tailored sweeps: Forbes, R. A.; Laukien, F. H.; Wronka, J. *Int. J. Mass Spectrom. Ion Processes* **1988**, *83*, 23.

(20) (a) Fisher, E. R.; Schultz, R. H.; Armentrout, P. B. ***J. Phys. Chem.*** **1989**, ***93***, 7382. (b) Schröder, D.; Hrušák, J.; Schwarz, H. *Ber. Bunsen-Ges. Phys. Chem.* **1993**, *97*, 1085.

(21) Schröder, D.; Schwarz, H. *Angew. Chem., Int. Ed. Engl.* **1990**, *29*, 1433.

(22) Schröder, D.; Schwarz, H.; Clemmer, D. E.; Chen, Y.-M.; Armentrout, P. B.; Baranov, V. I.; Böhme, D. K. *Int. J. Mass Spectrom. Ion Processes* **1997**, *161*, 175.

(23) (a) Su, T.; Chesnavich, W. J. *J. Chem. Phys.* **1982**, *76*, 5183. (b) Su, T. *J. Chem. Phys.* **1988**, *89*, 5355.

(24) (a) Schröder, D.; Hrušák, J.; Hertwig, R.; Koch, W.; Schwerdtfeger, P.; Schwarz, H. *Organometallics* **1995**, *14*, 312. (b) Dieterle, M.; Harvey, J. N.; Schröder, D.; Schwarz, H.; Heinemann, C.; Schwarz, J. *Chem. Phys. Lett.* **1997**, *277*, 399.

(25) The pressures have been corrected for the relative sensitivity of the ion gauge toward different gases: (a) Nakao, F. *Vakuum* **1975**, *25*, 431. (b) Bartmess, J. E.; Georgiadis, R. M. *Vacuum* **1983**, *33*, 149. (c) Schröder, D. Ph.D. Thesis, Technische Universität Berlin D83, 1992.

(26) (a) Lee, C.; Yang, W.; Parr, R. G. *Phys. Rev B* **1988**, *37*, 785. (b) Miehlich, B.; Savin, A.; Stoll, H.; Preuss, H. *Chem. Phys. Lett.* **1989**, *157*, 200. (c) Becke, A. D. *J. Chem. Phys.* **1993**, *98*, 5648.

(27) Frisch, M. J.; Trucks, G. W.; Schlegel, H. B.; Gill, P. M. W.; Johnson, B. G.; Robb, M. A.; Cheeseman, J. R.; Keith, T. A.; Petersson, G. A.; Montgomery, J. A.; Raghavachari, K.; Al-Laham, M. A.; Zakrzewski, V. G.; Ortiz, J. V.; Foresman, J. B.; Cioslowski, J.; Stefanov, B. B.; Nanayakkara, A.; Challacombe, M.; Peng, C. Y.; Ayala, P. Y.; Chen, W.; Wong, M. W.; Andres, J. L.; Replogle, E. S.; Gomperts, R.; Martin, R. L.; Fox, D. J.; Binkley, J. S.; Defrees, D. J.; Baker, J.; Stewart, J. P.; Head-Gordon, M.; Gonzalez, C.; Pople, J. A. *Gaussian 94* (Revision A.1); Gaussian Inc.: Pittsburgh, PA, 1995.

(28) (a) Glukhovtsev, M. N.; Bach, R. D.; Nagel, C. J. *J. Phys. Chem. A* **1997**, *101*, 316. (b) Kellogg, C. B.; Irikura, K. K. *J. Phys. Chem. A* **1999**, *103*, 1150.

(29) (a) Kappes, M. M.; Staley, R. H. *J. Phys. Chem.* **1981**, *85*, 942. (b) Schröder, D.; Fiedler, A.; Ryan, M. F.; Schwarz, H. *J. Phys. Chem.* **1994**, *98*, 68. (c) Clemmer, D. E.; Chen, Y.-M.; Khan, F. A.; Armentrout, P. B. *J. Phys. Chem.* **1994**, *98*, 6522. (d) Fiedler. A.; Schröder, D.; Shaik, S.; Schwarz, H. *J. Am. Chem. Soc.* **1994**, *116*, 10734. (e) Baranov, V.;

Jahavery, G.; Hopkinson, A. C.; Böhme, D. K. *J. Am. Chem. Soc.* **1995**, *117*, 12801. (f) Fiedler, A. Ph.D. Thesis, Technische Universität Berlin D83, 1996.

(30) (a) Elkind, J. L.; Armentrout, P. B. *J. Am. Chem. Soc.* **1986**, *108*, 2765. (b) Elkind, J. L.; Armentrout, P. B. *J. Phys. Chem.* **1986**, *90*, 5736.

(31) Schröder, D.; Kretzschmar, I.; Schwarz, H.; Rue, C.; Armentrout, P. B. *Inorg. Chem.*, in press.

(32) Brönstrup, M.; Kretzschmar, I.; Schröder, D.; Schwarz, H. *Helv. Chim. Acta* **1998**, *81*, 2348.

(33) Berkowitz, J.; Ellison, G. B.; Gutman D. *J. Phys. Chem.* **1994**, *98*, 2744

(34) Brönstrup, M.; Schröder, D.; Schwarz, H. *Chem. Eur. J.* **1999**, *5*, 1176.

(35) (a) Hildenbrand, D. L. *J. Chem. Phys.* **1995**, *103*, 2634. (b) Bach, R. D.; Shobe, D. S.; Schlegel, H. B.; Nagel, C. J. *J. Phys. Chem.* **1996**, *100*, 8770.

(36) Filatov, M.; Shaik, S. *J. Phys. Chem. A* **1998**, *102*, 3835.

(37) The error is estimated from the average deviations of the calculated heats of reaction for several model processes from known literature values. The reactions employed in this procedure are (a) $FeS^+ + H_2 \rightarrow Fe^+ (^4F) + H_2S$, (b) $Fe^+ (^6D) \rightarrow Fe^+ (^4F)$, (c) $FeS^+ (^6\Sigma^+) \rightarrow FeS^+ (^4\Pi)$, (d) $H_2S \rightarrow HS + H$, and (e) $FeH^+ + SH \rightarrow FeSH^+ + H$.

(38) See also: Hübner, O.; Termath, V.; Berning, A.; Sauer, J. *Chem. Phys. Lett.* **1998**, *294*, 37.

(39) Shaik, S.; Danovich, D.; Fiedler, A.; Schröder, D.; Schwarz, H. *Helv. Chim. Acta* **1995**, *78*, 1393.

(40) Hrušak, J.; Schröder, D.; Schwarz, H. *Chem. Phys. Lett.* **1994**, *225*, 416.

(41) Hoyan, S.; Ohanessian, G. *Chem. Phys. Lett.* **1997**, *280*, 266.

(42) (a) Newcomb, M.; Le Tadic, M.-H.; Putt, D. A.; Hollenberg, P. F. *J. Am. Chem. Soc.* **1995**, *117*, 3312. (b) Newcomb, M.; Le Tadic-Biadatti, M.-H.; Chestrey, D. L.; Roberts, E. S.; Hollenberg, P. F. *J. Am. Chem. Soc.* **1995**, *117*, 12085.

(43) Moore, C. E. *Atomic Energy Levels*; National Standard Ref. Data; National Bureau of Standards NSRDS-NBS 35; NBS: Washington, DC, 1971.

(44) (a) Gunnarson, O.; Jones, R. O. *Phys. Rev. B* **1985**, *31*, 7588. (b) Russo, T. V.; Martin, R. L.; Hay, P. J. *J. Chem. Phys.* **1994**, *101*, 7729. (c) Holthausen, M. C.; Heinemann, C.; Cornehl, H. H.; Koch, W.; Schwarz, H. *J. Chem. Phys.* **1995**, *102*, 4931. (d) Bauschlicher, C. W., Jr. *Chem. Phys.* **1996**, *211*, 163.

(45) As the nature of **3** is very much that of a simple electrostatic complex, the relative stabilities of **3** ($^4A''$) and **3** ($^6A''$) may well also be affected. This would place the sextet and quartet species very close in energy.

(46) (a) Ohanessian, G.; Goddard, W. A., III. *Acc. Chem. Res.* **1990**, *23*, 386. (b) Petterson, L. G. M.; Bauschlicher, C. W.; Langhoff, S. R.; Partridge, H. *J. Chem. Phys.* **1987**, *87*, 481. (c) Carter, E. A.; Goddard, W. A., III. *J. Phys. Chem.* **1988**, *92*, 5679.

(47) McKee, M. L. *J. Am. Chem. Soc.* **1990**, *112*, 2601.

(48) One may think of a third mechanism (see ref 36) where the dihydrogen approaches the FeS^+ in a collinear manner at the sulfur. Next, a hydrogen radical is transferred from the hydrogen molecule to the FeS^+ in a single step to yield $FeSH^+$ and H. In terms of the PES depicted in Figure 2, this is equivalent to entering the PES from the product side at the energy of $FeSH^+ + H$ with no barrier in excess of the reaction endothermicity. Thus, although possible, this mechanism cannot explain the delayed threshold observed for $FeSH^+$ and is therefore not considered any further.

(49) Shaik, S.; Filatov, M.; Schröder, D.; Schwarz, H. *Chem. Eur. J.* **1998**, *4*, 193.

(50) "Normal" refers to the default setting in Gaussian 94 (max. force = 0.000 45; RMS force = 0.000 30; max. displacement = 0.001 80; RMS displacement = 0.001 20), whereas "tight" convergence criteria correspond to max. force = 0.000 015, RMS force = 0.000 010, max. displacement = 0.000 060, and RMS displacement = 0.000 040.

(51) Tilson, J. L.; Harrison, J. F. *J. Phys. Chem.* **1992**, *96*, 1667

(52) Danovich, D.; Shaik, S. *J. Am. Chem. Soc.* **1997**, *119*, 1773.